

# Raman Scattering from High-Frequency Phonons in Supported *n*-Graphene Layer Films

A. Gupta,<sup>†</sup> G. Chen,<sup>†</sup> P. Joshi,<sup>‡</sup> S. Tadigadapa,<sup>‡</sup> and P.C. Eklund<sup>\*,†,§</sup>

*Department of Physics, Electrical Engineering, Materials Research Institute and  
Department of Materials Science and Engineering, The Pennsylvania State University,  
University Park, Pennsylvania 16802*

Received June 20, 2006; Revised Manuscript Received July 24, 2006

## ABSTRACT

Results of room-temperature Raman scattering studies of ultrathin graphitic films supported on Si (100)/SiO<sub>2</sub> substrates are reported. The results are significantly different from those known for graphite. Spectra were collected using 514.5 nm radiation on films containing from  $n = 1$  to 20 graphene layers, as determined by atomic force microscopy. Both the first- and second-order Raman spectra show unique signatures of the number of layers in the film. The *n*GL film analogue of the Raman G-band in graphite exhibits a Lorentzian line shape whose center frequency shifts linearly relative to graphite as  $\sim 1/n$  (for  $n = 1$   $\omega_G \approx 1587$  cm<sup>-1</sup>). Three weak bands, identified with disorder-induced first-order scattering, are observed at  $\sim 1350$ ,  $1450$ , and  $1500$  cm<sup>-1</sup>. The  $\sim 1500$  cm<sup>-1</sup> band is weak but relatively sharp and exhibits an interesting *n*-dependence. In general, the intensity of these D-bands decreases dramatically with increasing *n*. Three second-order bands are also observed ( $\sim 2450$ ,  $\sim 2700$ , and  $3248$  cm<sup>-1</sup>). They are analogues to those observed in graphite. However, the  $\sim 2700$  cm<sup>-1</sup> band exhibits an interesting and dramatic change of shape with *n*. Interestingly, for  $n < 5$  this second-order band is more intense than the G-band.

Several interesting reports of unusual electrical transport in thin graphite films have appeared recently.<sup>1–13</sup> These films comprise only a few atomic layers of sp<sup>2</sup>-bonded carbon known as “graphene” layers. Below, we refer to these unique atomically thin films as *n*-graphene layer films (i.e., *n*GL). Recently, bottom gate modulation of the current in the plane of the *n*GL film was also demonstrated which represents the first time that gate control of the current has been observed in a metallic or semimetallic system.<sup>5</sup> Interesting oscillatory magneto-transport phenomena sensitive to the shape of the Fermi surface<sup>1,4,6,7,9,10,12,14</sup> and an unusual half-integer quantum Hall effect have been reported.<sup>4,6,11,14,15</sup>

Crystalline graphite is a strongly anisotropic layered solid consisting of a periodic ...ABAB... stacking of graphene layers. All the formal chemical bonding in graphite is associated with the strong sp<sup>2</sup> intralayer bonds; these layers are, in turn, coupled by very weak van der Waals bonds. As a result of this strongly anisotropic bonding, weak (strong) electron and phonon dispersion is calculated<sup>16,17–28</sup> and observed<sup>29,30</sup> along the directions perpendicular (parallel) to the graphene planes. Any unique phonon character of supported *n*GL films is therefore expected to be due to the

importance of the reduction and/or eventual loss of these interlayer forces (i.e., at  $n = 1$ ) and to a combination of weak charge transfer and/or strain associated with the coupling of the film to the substrate.

Phonon and electronic state dispersion in a single graphene layer has been studied theoretically for many years.<sup>31–33</sup> In fact, these dispersion curves led to the prediction of chirality-dependent one-dimensional electronic and phonon dispersion in carbon nanotubes.<sup>17</sup> Experimental success in realizing well-ordered graphene (or *n*GLs) has been somewhat limited until very recently. A few years ago, a synthesis breakthrough was reported which is generally applicable to many layered solids that exhibit weak interlayer bonds (e.g., BN, NbSe<sub>2</sub>).<sup>34</sup> The approach relies on the careful mechanical transfer of a thin section of material from the outer basal plane surface of a parent crystal to a supporting substrate. In one case, this was elegantly accomplished by mounting a small graphite crystal on a tip-less cantilever held in an atomic force microscope (AFM).<sup>12</sup> Thin  $n \approx 3$  *n*GLs have also been fabricated by the preferential thermal evaporation of Si from the (0001) surface of SiC in ultrahigh vacuum, and they have been shown also to exhibit oscillatory magnetoresistance.<sup>1</sup>

Here we present the first formal report of our Raman scattering studies on *n*GLs, where *n* is in the range  $1 < n < 20$ , as determined by AFM.<sup>35</sup> The films were made by mechanically transferring thin flakes of material from highly oriented pyrolytic graphite (HOPG) on to a reasonably

\* To whom correspondence should be addressed. E-mail: pce3@psu.edu.

<sup>†</sup> Department of Physics.

<sup>‡</sup> Electrical Engineering.

<sup>§</sup> Materials Research Institute and Department of Materials Science and Engineering.

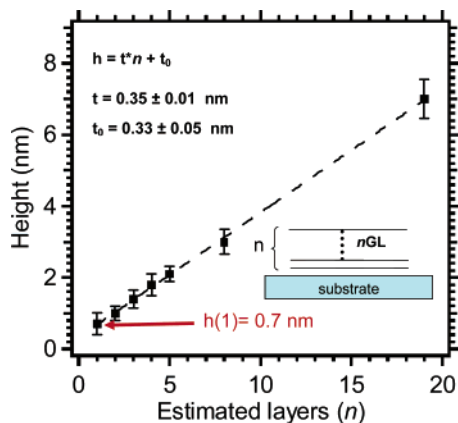


**Figure 1.** Effective  $n$ GL film height vs assigned  $n$ . The straight line is a least-square fit to the data. The apparent thickness of a graphene layer is  $t = 0.35 \pm 0.01$  nm, and the AFM offset parameter is  $t_0 = 0.33$  nm (see text for discussion).

smooth Si substrate. Despite the short range and weak interlayer forces within these films, we have observed a surprisingly continuous and systematic change in the first- and second-order high frequency intralayer phonons as the number of layers  $n$  in the film increases. Raman scattering can therefore be used to identify the number of layers in an  $n$ GL film.

Our films were prepared as follows. Thin basal plane sections were removed from large slabs ( $\sim 5 \times 5 \times 1$  mm<sup>3</sup>) of highly oriented pyrolytic graphite (HOPG)<sup>36,37</sup> by Scotch Tape (3M) and were transferred to Si (100) substrates. These substrates have a  $\sim 100$ -nm thick thermally grown oxide overlayer, such as typically used for bottom gate control of nanotubes and nanowire devices.<sup>38,39</sup> An atomic force microscope (AFM; model XE 100, PSIA, Inc.) operating under ambient conditions was used to measure the surface roughness of the substrate ( $\sim 1$ – $2$  nm) and the apparent thickness of the various  $n$ GL films studied here. Typical minimum lateral dimensions of these  $n$ GLs usually exceeded  $\sim 2$ – $4$   $\mu$ m. MicroRaman spectra could therefore be collected from a single  $n$ GL using a  $100\times$  objective with a spot size of  $\sim 1$   $\mu$ m. A variety of  $n$ GL flakes were deposited on a single Si substrate that was in turn mounted on the precision  $x$ – $y$  translation stage of our Raman microscope. Raman spectra were then collected using 514.5 nm excitation under ambient conditions at low laser power ( $<2$  mW) using a JY-ISA T64000 triple holographic grating spectrometer with an L-N<sub>2</sub>-cooled CCD detector. A low-pressure Hg lamp (Oriental) was set up in the background to provide in all spectra a reference frequency that is present as a narrow line at 1122.5 cm<sup>−1</sup>. The intrinsic resolution of the Raman spectrometer was also observed and recorded as the line shape of this Hg line. Specific  $n$ GLs that had been previously characterized by AFM (film thickness and basal plane shape) could be recognized in the video display of the Raman microscope by their characteristic irregular shape. In this way, we were able to collect Raman spectra of  $n$ GL films of known thickness ( $n$ ).

In Figure 1, we plot the measured AFM thickness ( $h$ ) vs our assigned value for  $n$ . The straight line is the result of a

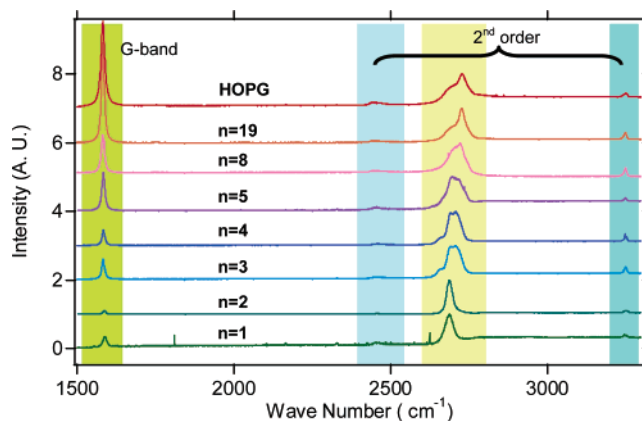


**Figure 2.** High-frequency first- and second-order microRaman spectra of  $n$ GL films supported on a SiO<sub>2</sub>/Si substrate and HOPG. The data were collected using 514.5 nm radiation under ambient conditions. The spectra are scaled to produce an approximate match in intensity for the  $\sim 2700$  cm<sup>−1</sup> band. Note: (1) the shape and frequency of this second-order band is sensitive to the number of layers  $n$ , and (2) the relative intensity of the second-order band at 2700 cm<sup>−1</sup> is larger than that of the first order-allowed G-band for  $n < 5$ .

linear least-squares fit to the data. In making the tentative assignment for  $n$ , we assumed that the film would have a thickness given by the linear relation  $h \approx n \cdot t + t_0$ , where  $n$  is an integer (number of layers),  $t$  is the approximate theoretical thickness of a graphene layer, and  $t_0$  is an instrumental offset (i.e., independent of  $n$ ). The data for  $h$  in Figure 1 represents the average step height obtained for a single  $n$ GL flake from averaging  $\sim 100$  individual line scans using a Si AFM cantilever. As can be seen, the linear fit to the  $h(n)$  data is very good and we obtain  $t = 0.35 \pm 0.01$  nm, in good agreement with  $c/2 = 0.335$  nm for graphite;<sup>16,17,40</sup> the offset obtained is  $t_0 = 0.33 \pm 0.05$  nm. We propose that  $t_0$  may be the result, in part, of a different force of attraction between the tip and graphene, as compared to the tip with SiO<sub>2</sub>. From the least-squares fit, we find that the  $n = 1$   $n$ GL has an apparent thickness of  $h(1) = (t + t_0) = 0.68 \pm 0.07$  nm.

In Figure 2, we show a series of high-frequency Raman spectra for  $n$ GLs of various  $n$  collected in a single experimental session. By this we mean that the spectra were collected in succession by only moving the  $x$ – $y$  stage to position a new  $n$ GL flake under the microscope objective. The spectra in Figure 2 cover the region,  $\sim 1500$ – $3600$  cm<sup>−1</sup>, and therefore contain contributions from both first-order scattering, i.e., the G-band ( $\sim 1582$  cm<sup>−1</sup> in graphite) and also second-order scattering. The Raman spectra have been stacked in the figure from bottom to top according to increasing  $n$ ; the spectrum of HOPG ( $n \approx \infty$ ) appears on top. Furthermore, the intensity of each spectrum in Figure 2 has been scaled to artificially produce the same-strength second-order band near  $\sim 2700$  cm<sup>−1</sup>. If plotted in absolute Raman scattering intensity units (e.g., counts W<sup>−1</sup> s<sup>−1</sup>), the true G-band intensity in Figure 2 would increase over the range  $n = 1$  to  $\sim 20$  almost linearly with the number of layers in the  $n$ GL. In most of our experiments (passes), the G-band for HOPG is comparable in intensity to that of  $n \approx 19$ ,

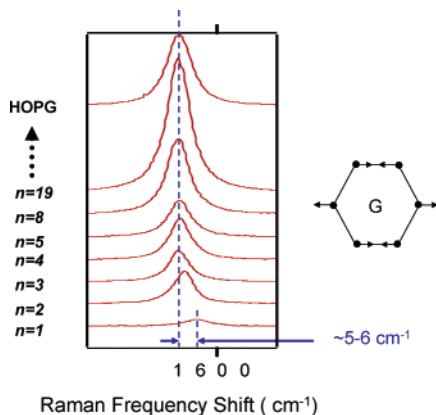


**Figure 3.** First order-allowed Raman G-band for supported  $n$ GL films vs number of layers  $n$ . The data were collected using 514.5 nm radiation under ambient conditions. The position of this band upshifts linearly, relative to graphite with increasing  $1/n$  (see Figure 4).

suggesting that the optical penetration depth in the  $n$ GL is  $\sim 20$  layers. Several general observations can easily be made from Figure 2: (1) the G-band frequency downshifts with increasing  $n$  (for small  $n$ ), (2) the second-order  $\sim 2700 \text{ cm}^{-1}$  band exhibits an interesting  $n$ -dependence in shape and frequency, (3) the sharp second-order feature at  $\sim 3248 \text{ cm}^{-1}$  is insensitive to  $n$ , (4) for  $n < 5$ , the second-order  $\sim 2700 \text{ cm}^{-1}$  band for an  $n$ GL is more intense than the first-order G-band, and (5) additional weak features are present in the first-order region ( $\omega < 1620 \text{ cm}^{-1}$ ) (we show these later on an expanded intensity scale).

In Figure 3, on an expanded frequency scale, we show the G-band for various  $n$ GLs. The spectra are stacked from bottom to top with increasing  $n$ . The spectra in the figure were also collected in a single pass; i.e. they were also collected sequentially under identical optical conditions. The Raman spectra in Figure 3 are not scaled, although the intensity of the HOPG G-band is less than that normally observed (the HOPG G-band intensity is typically comparable to  $n \approx 19$  data). As can be seen in the figure, the G-band clearly downshifts with increasing  $n$ . Careful Voigt line shape analyses of these G-bands show that they are extremely well fit by a single Lorentzian that has been “folded” with a Gaussian instrument function. The Gaussian is defined by the spectral shape of the low-pressure Hg line present in all our Raman spectra. Interestingly, the G-band frequency  $\omega_G$  exhibits an almost linear dependence on  $1/n$ , i.e.,  $\omega_G(n) = \omega_G(\infty) + \beta/n$ , where  $\beta \approx 5.5 \text{ cm}^{-1}$  is a constant. This behavior is shown in Figure 4 which presents the results of eight separate studies (passes) mostly, but not exclusively, obtained from the same set of  $n$ GLs. However, in each successive pass, a different location on the particular  $n$ GL was excited by the laser.

It is of interest to compare the value obtained for the G-band frequency of  $\text{SiO}_2$ -supported graphene, i.e.,  $\omega_G(1) = 1587 \text{ cm}^{-1}$  (Figure 4) to the strongest high-frequency first-order mode of moderate diameter (e.g.,  $D \approx 1.4 \text{ nm}$ ) single-walled carbon nanotubes (SWNT), e.g.,  $\omega \approx 1592 \text{ cm}^{-1}$ .<sup>16,17,41</sup> For SWNTs near this diameter (e.g.,  $1.2\text{--}1.6 \text{ nm}$ ), it is thought that the wall curvature of the nanotube does not

strongly effect the C–C intra-atomic force constants.<sup>17,42</sup> If we accept this point of view, then our value for  $\omega_G(n = 1) \approx 1587 \text{ cm}^{-1}$  is almost  $5 \text{ cm}^{-1}$  less than anticipated.

Our Voigt line shape analysis of the G-bands typically returned an uncertainty for the band frequency of only  $\sim 0.1\text{--}0.2 \text{ cm}^{-1}$ . Furthermore, absolute frequency calibration uncertainty in our experiments is small ( $\sim 0.1\text{--}0.2 \text{ cm}^{-1}$ ), as all G-band frequency scales are referenced to the nearby Hg line. Thus, it is somewhat surprising that the scatter in the frequency ( $\omega_G$ ) data (Figure 4) for fixed  $n$  is about twice as large as anticipated; i.e. the observed scatter is  $\sim \pm 0.5\text{--}1 \text{ cm}^{-1}$ . The larger scatter in  $\omega_G(n)$  data suggests that there may be a spot-to-spot variation within the  $n$ GL films. Perhaps this is due to the spectral difference produced by excitation near (or far) from a grain-boundary in the HOPG (the HOPG basal plane grain size is  $\sim 1\text{--}3 \mu\text{m}$  which is comparable to the laser spot diameter).

The symmetry and degeneracy of the long wavelength ( $q = 0$ ) optical phonons in graphite and graphene can be obtained by a group theoretical analysis. For graphite, with four atoms per primitive cell (two per layer in adjacent A and B layers), it has been shown that the atomic representation reduces to  $\Gamma_{\text{graphite}} = E_{2g}^{(1)} + E_{2g}^{(2)} + E_{1u} + A_{1u} + B_{1g}$ , where the E modes are doubly degenerate, and the A and B modes are singly degenerate. The  $E_{2g}$  symmetry modes are Raman-active ( $\omega(E_{2g}^{(1)}) = 42 \text{ cm}^{-1}$ ;  $\omega(E_{2g}^{(2)}) = 1582 \text{ cm}^{-1}$ ). The low-frequency  $E_{2g}^{(1)}$  modes can be identified with a rigid shearing of adjacent graphene layers.<sup>17</sup> The low frequency of this mode is a measure of the weak interlayer van der Waals forces. On the other hand, the high-frequency Raman-active  $E_{2g}^{(2)}$  modes and IR-active  $E_{1u}$  ( $1587 \text{ cm}^{-1}$ ) modes both involve a stretching of unusually strong *intralayer* bonds; therefore, only a small component of the mode-restoring force comes from *interlayer* bonds. The out-of-plane graphite  $A_{1u}$  ( $868 \text{ cm}^{-1}$ ) mode is IR-active, and the  $B_{1g}$  mode ( $127 \text{ cm}^{-1}$ ) is optically silent. Both the electronic states and the phonon states must depend, to some extent, on  $n$  in an  $n$ GL. Of course, the question remains: “How much do these states vary with  $n$  for small  $n$ , and with increasing  $n$ , by what value of  $n$  will the variation cease to be important?”

For the case of graphene, there are two atoms per primitive cell, and it can be easily shown that  $\Gamma_{\text{graphene}} = E_g + A_1 + B_1$ . In graphene, it can then be seen that several “graphitic” modes are lost; i.e. their re-appearance in an  $n$ GL requires at least a doubling of the number of layers ( $n = 2$ ) and an interlayer interaction. Several calculations of the phonon modes for graphene have appeared.<sup>31–33,43</sup> Unfortunately, to date, there have not been any experimental reports to test the subtle differences that can occur between the phonons in graphene and graphite. The phonon dispersion and corresponding one-phonon DOS for graphene calculated according to Mapeli and collaborators<sup>28</sup> appears in Figure 5. Particular attention in the figure should be paid to strong peaks in the DOS at  $\sim 1380$  and  $1600 \text{ cm}^{-1}$  and the weak peak at  $\sim 1500 \text{ cm}^{-1}$ . Evidence for structure in the first- and second-order Raman spectra associated with these maxima are seen, as discussed below.

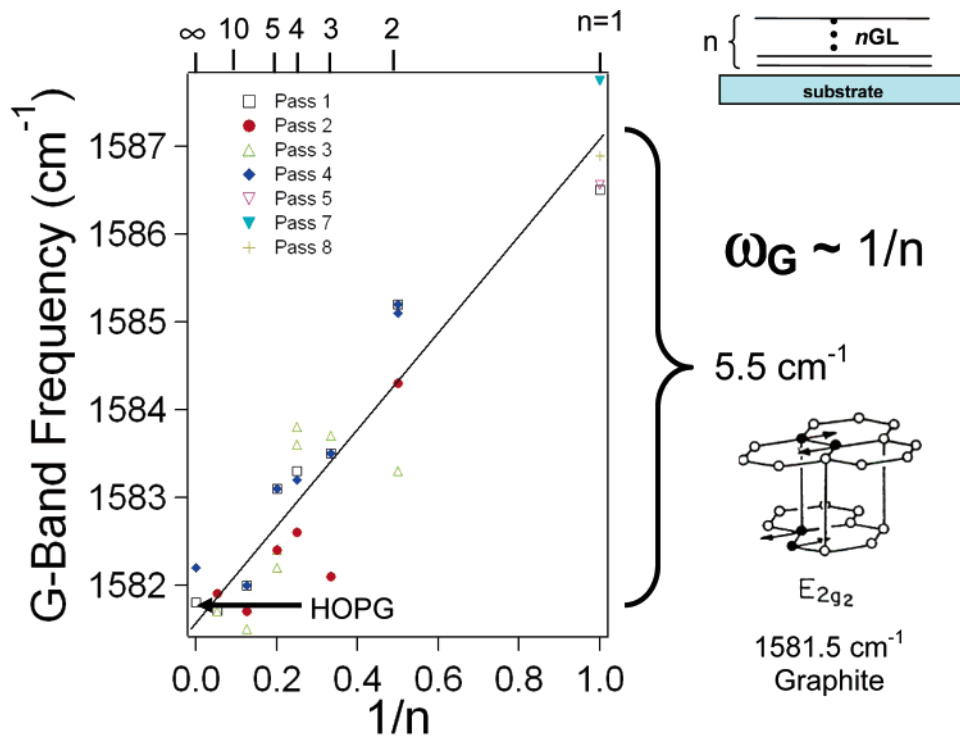


**Figure 4.** G-band frequency vs  $1/n$ . Each pass represents a set of data collected under identical optical conditions. The solid line represents the results of a least-squares fit to the data:  $\omega_G(\infty) = 1581.6 \text{ cm}^{-1}$  and  $d\omega/d(1/n) = 5.5 \text{ cm}^{-1}$ . The average of five values found for supported graphene ( $n = 1$ ) is  $\omega_G = 1587.1 \text{ cm}^{-1}$ .

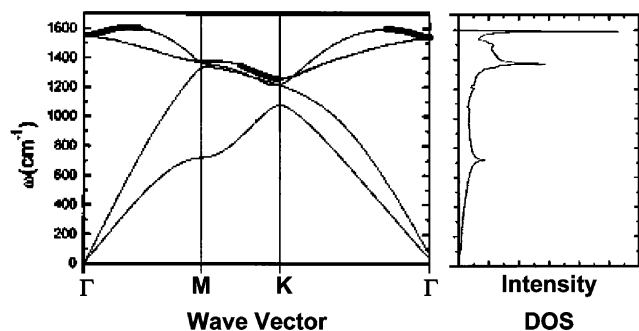


**Figure 5.** Calculated phonon dispersion curves and one-phonon density of states (DOS) for unsupported (free-standing) graphene by Mapeli et al.<sup>43</sup> Structure in the phonon DOS is expected in D- and second-order scattering.

From the symmetry analysis, it should be clear that the Raman band we observe in the interval  $\sim 1581\text{--}1588 \text{ cm}^{-1}$  in  $n$ GLs (Figures 2 and 3) should be connected with the  $E_{2g}^{(2)}$  modes of graphite (G-band), as perturbed by the small number of layers in the film and the coupling of the film to the substrate. However, the one-phonon scattering symmetry analysis does not allow for the weak Raman bands that we observe in  $n$ GLs near  $\sim 1350$ ,  $1450$ , and  $1500 \text{ cm}^{-1}$ . These weak Raman bands can be seen in Figure 6, where we have considerably expanded the intensity so that the G-band maxima are way off-scale. The strongest band in the figure ( $\sim 1350 \text{ cm}^{-1}$ ) is identified with a “disorder”-induced band or “D-band”, as it is known in the literature, that has been observed in many  $sp^2$ -bonded carbons. These studies have shown that the Raman D-band intensity and position, respectively, depend on the degree and nature of the basal

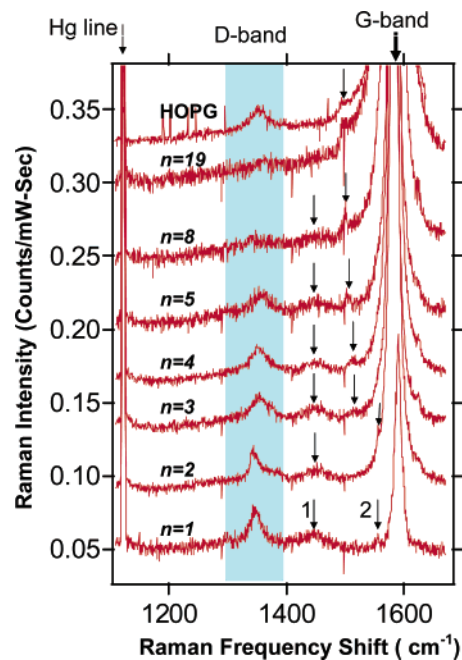


**Figure 6.** Raman spectra (expanded intensity scale) of supported  $n$ GL films and HOPG in the vicinity of the G-band. The spectra have been arbitrarily displaced in the vertical direction for clarity. The data were collected using  $514.5 \text{ nm}$  radiation under ambient conditions. The spectra have been scaled to show the weak structure which has been identified with the one-phonon DOS in Figure 5. The arrows in the figure identify weak scattering features. ( $D_2$  and  $D_3$  correspond, respectively, to arrow 1 and 2.) Note that the  $D_3$  feature at  $\sim 1500 \text{ cm}^{-1}$  is sensitive to the number of layers  $n$ .

plane disorder and the excitation wavelength.<sup>17,28,44–49</sup> For the  $n = 1$   $n$ GL (Figure 6), we observe that the D-band



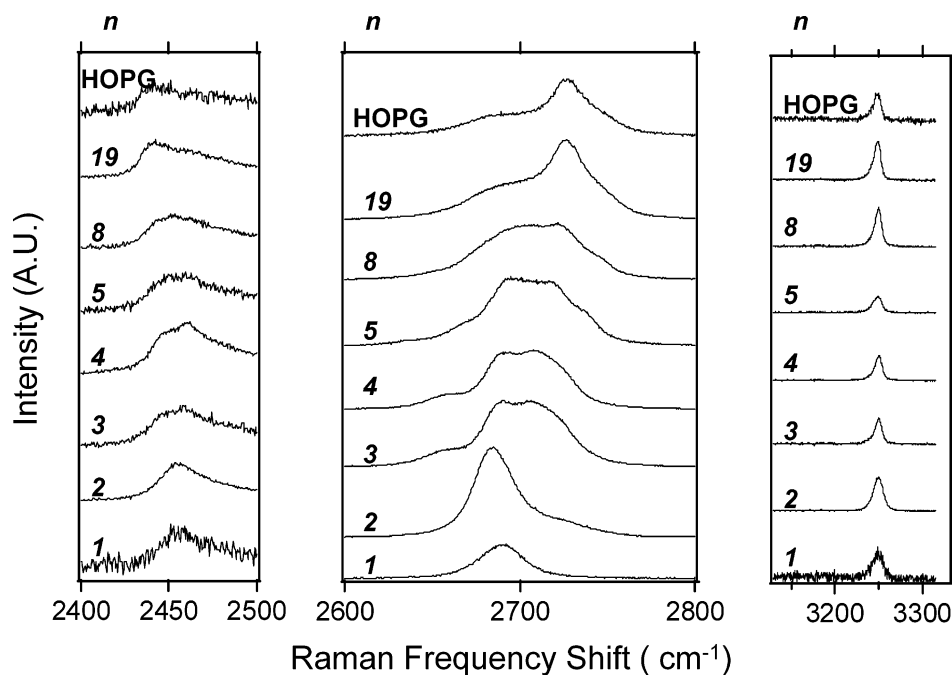


**Figure 7.** Second-order Raman spectra of supported  $n$ GL films. The data were collected using 514.5 nm radiation under ambient conditions. The spectra in each panel have been scaled to generate features of approximately the same height. These second-order bands also appear in Figure 2 which indicates their approximate relative scattering intensity to the G-band. Note that the  $\sim 2700\text{ cm}^{-1}$  band is sensitive to the number of layers  $n$ .

intensity  $I_D$  of the  $\sim 1350\text{ cm}^{-1}$  band is  $\sim 1/5$  of that of the G-band ( $I_G$ ). However, with increasing  $n$ , the D-band intensity  $I_D$  can be seen to dramatically decline relative to  $I_G$ . We observe that the intensity ratio ( $I_D/I_G$ ) exhibits an approximately exponential decline with increasing  $n$ . In addition to the  $\sim 1350\text{ cm}^{-1}$  D-band, two additional weak bands are observed that are also assigned to disorder-induced first-order scattering or “D-scattering”: ( $D_2$ )  $\approx 1450\text{ cm}^{-1}$  and ( $D_3$ )  $1500\text{ cm}^{-1}$ . It should be noted that the graphene phonon calculations of Mapeli et al. predict a weak but sharp DOS peak at  $\sim 1500\text{ cm}^{-1}$ . This  $1500\text{ cm}^{-1}$  peak is particularly interesting in that it has striking  $n$ -dependence, whereas the other D-scattering peaks (e.g.,  $D_2 \approx 1350\text{ cm}^{-1}$  and  $D_3 \approx 1450\text{ cm}^{-1}$ ) are largely insensitive to  $n$ .

It is also interesting to speculate about the origin of the  $n$ -dependence of the D-band scattering in  $n$ GLs. One explanation that we might offer for this observation is a bending of the graphene layers necessary to accommodate the surface roughness of the substrate. This view is motivated by the fact that our  $\text{SiO}_2/\text{Si}$  substrates are not atomically smooth. Our AFM measurements indicate a substrate roughness of  $\sim 1\text{--}2\text{ nm}$ , i.e.,  $\sim 3\text{--}6$  graphene layers. The  $n$ -dependence of the D-scattering then may stem from the loss in  $\text{sp}^2$  bond-bending disorder associated with the increase in rigidity of the  $n$ GL as the number of layers  $n$  increases. This cooperative (multilayer) film rigidity is expected to resist the deformation from planarity as the film, via a van der Waals coupling between substrate and  $n$ GL, attempts to conform to the underlying substrate roughness. That is, an  $n = 1$   $n$ GL is relatively very compliant and bends easily, while an  $n = 5$   $n$ GL should be much more rigid. Our suggestion of a planar deformation to induce D-band scattering, although novel, is consistent with the general

concept that many different mechanisms that break the translational symmetry of the basal plane can give rise to D-band scattering (e.g., finite basal plane size, boron-doping, bond-disorder, etc.).<sup>28,44–50</sup> Further work will be needed to confirm that variable film rigidity is responsible for the D-band scattering. This idea could be experimentally tested by studying films supported on atomically smooth substrates (e.g., mica) or suspended over a small hole in a substrate.

In Figure 7, we display in three separate panels, the second-order features shown in Figure 2, but on an expanded intensity scales. For clarity, the spectra are normalized to give them all approximately the same intensity, independent of  $n$ . The panels each display the evolution ( $n = 1$  (bottom) to HOPG (top)) of one of the three second-order bands observed at:  $\sim 2450\text{ cm}^{-1}$  (weak intensity),  $\omega(2D') \sim 2700\text{ cm}^{-1}$  (moderate to strong intensity), and  $\omega(2G') \sim 3248\text{ cm}^{-1}$  (moderate intensity). Based on the peaks in the phonon DOS of Mapeli et al. (Figure 5), the  $\sim 2450\text{ cm}^{-1}$  and  $\sim 2700\text{ cm}^{-1}$  bands must be due to combination scattering, i.e.,  $(\omega_1 + \omega_2)$ , while the relatively narrow second-order band at  $\sim 3248\text{ cm}^{-1}$  must be a  $2\omega$  feature (overtone scattering) associated with a doubling of the highest phonon frequency in the zone. It is interesting that, although we observe that the G-band ( $q = 0$  mode of this optical branch) upshifts with decreasing  $n$ , the maximum frequency of the same branch  $\omega(\text{max}) = 1/2\omega(2G')$  remains fixed in frequency. This result, among other experimental observations presented here, seems to be a good test for future lattice dynamics models of  $n$ GLs and supported  $n$ GLs.

In summary, we have prepared a variety of ultrathin graphitic films (or  $n$ GLs) by mechanical transfer from an HOPG slab to a  $\text{SiO}_2/\text{Si}$  substrate. The film thickness of

various  $n$ GL flakes was measured by averaging AFM  $z$ -scans. They exhibited lateral dimensions on the order of  $\sim 2\text{--}5\ \mu\text{m}$ . The effective film thickness data  $h$  vs assigned  $n$  was found to be well fit to a straight line, yielding the value  $t = 0.355$  for the thickness of a graphene layer, a little larger than  $c/2$  for graphite, but within experimental error. MicroRaman spectra were then collected on these films and correlated with the integer number of graphene layers per film. Surprisingly, despite the anticipated short range of the  $c$ -axis forces in graphite, the Raman spectra of  $n$ GLs were found to be very sensitive to  $n$ , for  $n$  as large as  $n = 10$ . Strong signatures of the number of graphene layers per film are seen in the weak  $D_3$ -scattering peak at  $\sim 1500\ \text{cm}^{-1}$ , in the position of the G-band, and in the second-order band observed near  $\sim 2700\ \text{cm}^{-1}$ . Detailed lattice dynamics calculations should be carried out on atomically thin films (vs  $n$ ) to understand how the subtle changes we observe in zone-center, mid-zone, and zone-edge modes affect the D, first-, and second-order scattering. It will also be necessary to extend these experimental studies to other excitation wavelengths ( $\lambda_{\text{ex}}$ ) to see which of these Raman bands are dispersive (i.e., the position of dispersive Raman bands depends on  $\lambda_{\text{ex}}$ ). The simple  $1/n$  behavior of the G-band position also remains unexplained. It is not known to what extent the  $1/n$  dependence is connected to strain (via coupling to the substrate) or to the finite number  $n$  of C-layers in the film.

Finally, the  $n$ GL D-band scattering intensity ( $\sim 1350\ \text{cm}^{-1}$ ) is observed to strongly decrease with increasing  $n$ . We have proposed that this behavior might correlate with the rigidity of the film and its ability to avoid distortion to accommodate the substrate roughness.

**Acknowledgment.** This work was supported, in part, by Penn State Materials Research Institute and the Penn State MRSEC under NSF Grant DMR 0213623. We acknowledge useful discussion with Dr. Humberto R. Gutierrez (Penn State) and Cynthia Coggins (PSIA, Inc.)

## References

- Berger, C.; Song, Z.; Li, T.; Li, X.; Ogbazghi, A. Y.; Feng, R.; Dai, Z.; Marchenkov, A. N.; Conrad, E. H.; First, P. N.; de Heer, W. A. Ultrathin epitaxial graphite: two-dimensional electron gas properties and a route toward graphene-based nanoelectronics. *J. Phys. Chem. B* **2004**, *108* (52), 19912.
- Bunch, J. S.; Yaish, Y.; Brink, M.; Bolotin, K.; McEuen, P. L., Coulomb oscillations and Hall effect in quasi-2D graphite quantum dots. *Nano Lett.* **2005**, *5* (2), 287.
- Dujardin, E.; Thio, T.; Lezec, H.; Ebbesen, T. W. Fabrication of mesoscopic devices from graphite microdisks. *Appl. Phys. Lett.* **2001**, *79* (15), 2474.
- Novoselov, K. S.; Geim, A. K.; Morozov, S. V.; Jiang, D.; Katsnelson, M. I.; Grigorieva, I. V.; Dubonos, S. V.; Firsov, A. A. Two-dimensional gas of massless Dirac fermions in graphene. *Nature (London)* **2005**, *438* (7065), 197.
- Novoselov, K. S.; Geim, A. K.; Morozov, S. V.; Jiang, D.; Zhang, Y.; Dubonos, S. V.; Grigorieva, I. V.; Firsov, A. A., Electric field effect in atomically thin carbon films. *Science* **2004**, *306* (5696), 666.
- Novoselov, K. S.; McCann, E.; Morozov, S. V.; Falko, V. I.; Katsnelson, M. I.; Geim, A. K.; Schedin, F.; Jiang, D. Unconventional quantum Hall effect and Berry's phase of  $2\pi$  in bilayer graphene. *Los Alamos National Laboratory, Preprint Archive, Condensed Matter* **2006**, 1.
- Ohashi, Y.; Yamamoto, K.; Kubo, T. Shubnikov-de Haas effect of very thin graphite crystals. *Carbon'01, An International Conference on Carbon, Lexington, KY, United States, July 14–19, 2001* **2001**, 568.
- Ohashi, Y.; Kubo, T. Magnetoresistance effect of thin films made of single graphite crystal. *Tanso* **2000**, *195*, 410.
- Rollings, E.; Gweon, G. H.; Zhou, S. Y.; Mun, B. S.; Hussain, B. S.; Fedorov, A. V.; First, P. N.; de Heer, W. A.; Lanzara, A. Synthesis and characterization of atomically-thin graphite films on a silicon carbide substrate. *Los Alamos National Laboratory, Preprint Archive, Condensed Matter* **2005**, 1.
- Zhang, Y.; Jiang, Z.; Small, J. P.; Purewal, M. S.; Tan, Y. W.; Fazlollahi, M.; Chudow, J. D.; Jaszczak, J. A.; Stormer, H. L.; Kim, P. Landau level splitting in graphene in high magnetic fields. *Los Alamos National Laboratory, Preprint Archive, Condensed Matter* **2006**, 1.
- Zhang, Y.; Tan, Y.-W.; Stormer, H. L.; Kim, P. Experimental observation of the quantum Hall effect and Berry's phase in graphene. *Nature (London, United Kingdom)* **2005**, *438* (7065), 201.
- Zhang, Y. B.; Small, J. P.; Amori, M. E. S.; Kim, P. Electric field modulation of galvanomagnetic properties of mesoscopic graphite. *Phys. Rev. Lett.* **2005**, *94* (17), 176803/1.
- Zhang, Y. B.; Small, J. P.; Pontius, W. V.; Kim, P. Fabrication and electric-field-dependent transport measurements of mesoscopic graphite devices. *Appl. Phys. Lett.* **2005**, *86* (7), 073104.
- Morozov, S. V.; Novoselov, K. S.; Schedin, F.; Jiang, D.; Firsov, A. A.; Geim, A. K. Two-dimensional electron and hole gases at the surface of graphite. *Phys. Rev. B: Condens. Matter Mater. Phys.* **2005**, *72* (20), 201401/1.
- Gusynin, V. P.; Sharapov, S. G. Unconventional Integer Quantum Hall Effect in Graphene. *Phys. Rev. Lett.* **2005**, *95* (14), 146801/1.
- Dresselhaus, M. S.; Dresselhaus, G.; Eklund, P. C., Eds. *Science of Fullerenes and Carbon Nanotubes*; Academic Press: San Diego, CA, 1996; p 965.
- Dresselhaus, M. S.; Eklund, P. C. Phonons in carbon nanotubes. *Adv. Phys.* **2000**, *49* (6), 705.
- Chico, L.; Perez-Alvarez, R.; Cabrillo, C. Low-frequency phonons in carbon nanotubes: A continuum approach. *Phys. Rev. B: Condens. Matter Mater. Phys.* **2006**, *73* (7).
- Maultzsch, J.; Reich, S.; Schlecht, U.; Thomsen, C. High-energy phonon branches of an individual metallic carbon nanotube. *Phys. Rev. Lett.* **2003**, *91* (8).
- Maultzsch, J.; Reich, S.; Thomsen, C.; Dobardzic, E.; Milosevic, I.; Damjanovic, M., Phonon dispersion of carbon nanotubes. *Solid State Commun.* **2002**, *121* (9–10), 471.
- Maultzsch, J.; Reich, S.; Thomsen, C.; Reuquardt, H.; Ordejon, P. Phonon dispersion in graphite. *Phys. Rev. Lett.* **2004**, *92* (7).
- Saito, R.; Jorio, A.; Souza, A. G.; Dresselhaus, G.; Dresselhaus, M. S.; Pimenta, M. A. Probing phonon dispersion relations of graphite by double resonance Raman scattering. *Phys. Rev. Lett.* **2002**, *88* (2).
- Saito, R.; Takeya, T.; Kimura, T.; Dresselhaus, G.; Dresselhaus, M. S. Raman intensity of single-wall carbon nanotubes. *Phys. Rev. B* **1998**, *57* (7), 4145.
- Wirtz, L.; Rubio, A. The phonon dispersion of graphite revisited. *Solid State Commun.* **2004**, *131* (3–4), 141.
- Yu, J.; Kalia, R. K.; Vashishta, P. Phonons in Graphitic Tubules - a Tight-Binding Molecular-Dynamics Study. *J. Chem. Phys.* **1995**, *103* (15), 6697.
- Zolyomi, V.; Kurti, J.; Gruneis, A.; Kuzmany, H. Origin of the fine structure of the Raman D band in single-wall carbon nanotubes. *Phys. Rev. Lett.* **2003**, *90* (15).
- Aljishi, R.; Dresselhaus, G. Lattice-Dynamical Model for Graphite. *Phys. Rev. B* **1982**, *26* (8), 4514.
- Ferrari, A. C.; Robertson, J. Interpretation of Raman spectra of disordered and amorphous carbon. *Phys. Rev. B* **2000**, *61* (20), 14095.
- Nicklow, R.; Smith, H. G.; Wakabaya, N. Lattice-Dynamics of Pyrolytic-Graphite. *Phys. Rev. B* **1972**, *5* (12), 4951.
- Nicklow, R.; Wakabaya, N.; Smith, H. G. Lattice Dynamics of Pyrolytic Graphite. *Bull. Am. Phys. Soc.* **1970**, *15* (3), 383.
- Yanagisawa, H.; Tanaka, T.; Ishida, Y.; Matsue, M.; Rokuta, E.; Otani, S.; Oshima, C. Analysis of phonons in graphene sheets by means of HREELS measurement and ab initio calculation. *Surf. Interface Anal.* **2005**, *37* (2), 133.
- Popov, V. N.; Lambin, P. Radius and chirality dependence of the radial breathing mode and the G-band phonon modes of single-walled carbon nanotubes. *Phys. Rev. B: Condens. Matter Mater. Phys.* **2006**, *73* (8), 085407.
- Saito, R.; Takeya, T.; Kimura, T.; Dresselhaus, G.; Dresselhaus, M. S. Finite-size effect on the Raman spectra of carbon nanotubes. *Phys. Rev. B* **1999**, *59* (3), 2388.

- (34) Novoselov, K. S.; Jiang, D.; Schedin, F.; Booth, T. J.; Khotkevich, V. V.; Morozov, S. V.; Geim, A. K. Two-dimensional atomic crystals. *Proc. Natl. Acad. Sci. U.S.A.* **2005**, *102* (30), 10451.
- (35) Gupta, A.; Joshi, P.; Eklund, P. C. In *Raman Scattering from Few-Layer Graphene Films*, 2006; APS March Meeting, Baltimore, MD, 2006; Baltimore, MD.
- (36) Moore, A. W. Properties and applications of highly oriented pyrolytic graphite - a review. *Extended Abstracts and Program - Biennial Conference on Carbon* **1979**, *14*, 203.
- (37) Moore, A. W. Highly oriented pyrolytic graphite. *Chem. Phys. Carbon* **1973**, *11*, 69.
- (38) Xiang, J.; Lu, W.; Hu, Y. J.; Wu, Y.; Yan, H.; Lieber, C. M. Ge/Si nanowire heterostructures as high-performance field-effect transistors. *Nature* **2006**, *441* (7092), 489.
- (39) Tans, S. J.; Verschuere, A. R. M.; Dekker, C. Room-temperature transistor based on a single carbon nanotube. *Nature* **1998**, *393* (6680), 49.
- (40) Kelly, B. T. *Physics of Graphite*; Applied Science: London, 1981.
- (41) Rao, A. M.; Richter, E.; Bandow, S.; Chase, B.; Eklund, P. C.; Williams, K. A.; Fang, S.; Subbaswamy, K. R.; Menon, M.; Thess, A.; Smalley, R. E.; Dresselhaus, G.; Dresselhaus, M. S. Diameter-selective Raman scattering from vibrational modes in carbon nanotubes. *Science* **1997**, *275* (5297), 187.
- (42) Jishi, R. A.; Venkataraman, L.; Dresselhaus, M. S.; Dresselhaus, G. Phonon Modes in Carbon Nanotubes. *Chem. Phys. Lett.* **1993**, *209* (1-2), 77.
- (43) Mapelli, C.; Castiglioni, C.; Zerbi, G.; Mullen, K. Common force field for graphite and polycyclic aromatic hydrocarbons. *Phys. Rev. B* **1999**, *60* (18), 12710.
- (44) Brown, S. D. M.; Jorio, A.; Dresselhaus, M. S.; Dresselhaus, G. Observations of the D-band feature in the Raman spectra of carbon nanotubes. *Phys. Rev. B: Condens. Matter Mater. Phys.* **2001**, *64* (7), 073403.
- (45) Dresselhaus, M. S.; Dresselhaus, G.; Jorio, A.; Souza, A. G.; Pimenta, M. A.; Saito, R. Single nanotube Raman spectroscopy. *Acc. Chem. Res.* **2002**, *35* (12), 1070.
- (46) Jorio, A.; Pimenta, M. A.; Fantini, C.; Souza, M.; Souza, A. G.; Samsonidze, G. G.; Dresselhaus, G.; Dresselhaus, M. S.; Saito, R. Advances in single nanotube spectroscopy: Raman spectra from cross-polarized light and chirality dependence of Raman frequencies. *Carbon* **2004**, *42* (5-6), 1067.
- (47) Liu, C. P.; Ding, J. W. Electronic structure of carbon nanotube: the roles of curvature, hybridization, and disorder. *J. Phys. Condens. Matter* **2006**, *18* (16), 4077.
- (48) Moradian, R. Disordered carbon nanotube alloys in the effective-medium supercell approximation. *Physical Review B* **2004**, *70* (20).
- (49) Pimenta, M. A.; Jorio, A.; Brown, S. D. M.; Souza, A. G.; Dresselhaus, G.; Hafner, J. H.; Lieber, C. M.; Saito, R.; Dresselhaus, M. S. Diameter dependence of the Raman D-band in isolated single-wall carbon nanotubes. *Phys. Rev. B* **2001**, *64* (4).
- (50) Dresselhaus, M. S.; Dresselhaus, G.; Pimenta, M. A.; Eklund, P. C. Raman Scattering in Carbon Materials. In *Analytical Applications of Raman Spectroscopy*; Pelletier, M. J., Ed.; Blackwell Science Ltd.: Oxford, UK, 1999; pp 367.

NL061420A